Neuro-Oncology Advances
5(1), 1–11, 2023 | https://doi.org/10.1093/noajnl/vdad042 | Advance Access date 11 April 2023

The brain-penetrant cell-cycle inhibitor p28 sensitizes brain metastases to DNA-damaging agents

Sunam Mander, Gregory S. Gorman, Lori U. Coward, Konstantin Christov, Albert Green, Tapas K. Das Gupta, and Tohru Yamada

Department of Surgery, Division of Surgical Oncology, University of Illinois College of Medicine, Chicago, Illinois, USA(S.M., K.C., A.G., T.K.D.G., T.Y.); McWhorter School of Pharmacy, Pharmaceutical, Social and Administrative Sciences, Samford University, Birmingham, Alabama 35229, USA(G.S.G., L.U.C.); Richard and Loan Hill Department of Biomedical Engineering, University of Illinois College of Engineering, Chicago, Illinois, USA(T.Y.)

Corresponding Author: Tohru Yamada, PhD, Department of Surgery, Division of Surgical Oncology, University of Illinois College of Medicine, Chicago, Illinois, USA(tohru@uic.edu).

Abstract

Background. Brain metastases (BMs), the most common tumors of the central nervous system, are life-threatening with a dismal prognosis. The major challenges to developing effective treatments for BMs are the limited abilities of drugs to target tumors and to cross the blood-brain barrier (BBB). We aimed to investigate the efficacy of our therapeutic approach against BMs in mouse models that recapitulate the clinical manifestations of BMs.

Methods. BMs mouse models were constructed by injecting human breast, lung cancer, and melanoma intracardially, which allowed the BBB to remain intact. We investigated the ability of the cell-penetrating peptide p28 to cross the BBB in an in vitro 3D model and in the BMs animal models. The therapeutic effects of p28 in combination with DNA-damaging agents (radiation and temozolomide) on BMs were also evaluated.

Results. p28 crossed the intact BBB more efficiently than the standard chemotherapeutic agent, temozolomide. Upon crossing the BBB, p28 localized preferentially to tumor lesions and enhanced the efficacy of DNA-damaging agents by activating the p53-p21 axis. In the BMs animal models, radiation in combination with p28 significantly reduced the tumor burden of BMs.

Conclusions. The cell-cycle inhibitor p28 can cross the BBB localize to tumor lesions in the brain and enhance the inhibitory effects of DNA-damaging agents on BMs, suggesting the potential therapeutic benefits of this molecule in BMs.

Key Points

1. The cell-penetrating peptide p28 crosses the intact blood-brain barrier.
2. p28 preferentially localizes to tumor lesions in the brain.
3. Through regulation of the cell cycle and apoptosis pathways, p28 in combination with DNA-damaging agents exerts therapeutic effects on brain metastases.

Brain metastases (BMs) refer to the development of intracranial tumors by circulating tumor cells derived from primary cancers outside the central nervous system (CNS)[1] and occur in 10%–30% of adults with cancer.[2,3] The development of BMs is a complex process, requiring primary cancer cell invasion into surrounding tissues and vessels, extravasation through the circulatory system, and growth in the brain.[1] BMs occur most commonly in patients with melanoma, breast cancer, and lung cancer, which account for 67%–80% of BMs cases.[4] The incidence of BMs is increasing, possibly due in part to advances in the efficacy of therapies that have increased the survival and improved the prognosis of patients with cancer.[5] Standard approaches for the management of BMs are continuing to improve, and current therapies include surgical

Importance of the Study

Despite recent medical advances, brain metastases (BMs) remain a clinical challenge. In this study, mouse models that mimic the clinical manifestations of BMs were used to test our approach against BMs. For that, the BM mouse models were generated by intracardial injections of breast cancer, lung cancer, and melanoma, the most common cancer types that cause BMs. The BMs mouse models have the intact blood-brain barrier (BBB), unlike the stereotactic injection method. With the in vitro 3D BBB model and the BMs mouse models, p28, a cell-penetrating peptide, was found to cross the BBB and accumulate in BMs lesions. Upon entry, cell-cycle inhibitor p28 enhances the efficacy of DNA-damaging agents such as radiation and temozolomide. These results provide a clear rationale for the use of combination approaches involving the brain-penetrant molecule p28 for the treatment of BMs.

resection, stereotactic radiosurgery, and whole-brain radiation therapy.[6,7] Recent advances in systemic chemotherapy, including molecular targeted therapy, have substantially improved the survival of patients, including those with BMs.[8,9] However, systemic administration of cytotoxic agents still plays a limited role in CNS diseases due to challenges related to delivery across the blood-brain barrier (BBB) to sites of metastasis in the brain.[10]

One promising approach for delivering therapeutics to the brain is the use of BBB-penetrating peptides capable of transporting neurotherapeutic cargo such as proteins, genetic material, and drugs across the brain parenchyma.[11,12] Some peptides transport cargo by binding receptors expressed on the luminal side of the brain with high affinity, whereas others penetrate the BBB via a receptor-independent mechanism[13,14] and are termed cell-penetrating peptides.[14–16] The straightforward synthesis of cell-penetrating peptides and their good biocompatibility and efficient tissue penetration represent advantages over other delivery vehicles.[17–19] We have studied the CPP p28, which comprises 28 amino acids of the protein azurin, a member of the cupredoxin family secreted from the opportunistic pathogen *Pseudomonas aeruginosa*.[20,21] p28 preferentially enters various types of cancer cells (eg, breast cancer, melanoma, lung cancer, and glioblastoma cells) compared to normal counterparts, reduces the proteasomal degradation of p53, and induces cell-cycle arrest at the G_2-M transition.[22–24] Importantly, p28 has no immunogenicity or cellular toxicity, as demonstrated in 2 phase I clinical trials, one in patients with advanced solid tumors (NSC745104) and the other in pediatric patients with recurrent/refractory CNS tumors (NCT01975116).[25–27]

In the development of systemic therapies for BMs, appropriate models are necessary to obtain insight into the mechanisms underlying the development of metastatic disease and to screen clinically relevant therapeutics. A variety of injection routes can be used to generate BMs animal models. They include intravenous injections, orthotopic injections, or intracardiac injections of cancer cells.[28] BMs models constructed by intravenous tail vein injection are typically avoided, as this approach leads primarily to metastases in other sites (eg, lung) prior to the brain.[29,30] The principal advantage of stereotactic orthotopic injection is the high success rate of inducing BMs,[31,32] but this approach disrupts BBB integrity and can alter the permeability of tumor lesions to drugs.[33,34] In contrast, intracardiac injection of cancer cells can produce BMs without disrupting the BBB.[35] Unlike stereotactic injection, intracardiac injection requires cancer cells to cross the BBB to induce BMs. Given that the loss of BBB integrity limits the ability of a model to recapitulate the clinically relevant characteristics of BMs,[36,37] it is important to use appropriate experimental models to investigate new therapeutics for BMs.

In this study, we examined the ability of p28 to cross the BBB in an in vitro 3D model and in animal models of BMs. We also investigate the efficacy of our therapeutic approach against BMs in the mouse model of BMs. To accomplish this, we utilized BMs mouse models based on the intracardiac injection of melanoma, breast cancer, and lung cancer cells. This model better recapitulates the biological features of metastases than classical models constructed by xenograft-based stereotactic injection approaches, which impair the BBB. Together, the findings that the cell-cycle inhibitor p28 can cross the BBB, localize to tumor lesions in the brain and enhance the antitumor effects of DNA-damaging agents on BMs suggest that this molecule has potential therapeutic effects against BMs.

Materials and Methods

Peptide Synthesis

p28 peptide (LSTAA DMQGV VTDGM ASGLD KDYLK PDD, 2914 Da) and Scrambled-p28 (Scr, GDLSA DMPLD MGKVT VSGLD YAQAD TDK, 2914 Da) were synthesized by CS Bio, Inc at >97% purity.

Cell Culture

A549 human lung cancer cells, MCF10A, and fibroblasts were purchased from American Type Culture Collection. UISO-Mel-7 melanoma[38] and UISO-BCA-1 breast cancer[39] cells were established in our laboratory. Brain-specific metastatic MDA-MB-231 (MDA-231BR) cells were a kind gift from Dr. T. Yoneda, The University of Texas Health Science Center at San Antonio. All cells were cultured at 37°C in a humidified chamber containing 5% CO_2.

In Vitro BBB Permeability Assay

Permeability to temozolomide (TMZ, Teva Pharmaceuticals, USA, #NDC 0093-7600-57) and p28 (CS Bio, CA) was assessed with 3D Human Blood-Brain Barrier Kits (Alphabioregen, #EP010) following the manufacturer's instructions. Briefly, the BBB models were thawed in BBB growth medium (#BBB-GM001), incubated overnight with fresh BBB growth medium, and then incubated with Endo-Neuro Pharmaceuticals media (#NMBBB001) for 3 days to establish a viable barrier. Following this step, 10 μM p28 and 100 μM TMZ were prepared in assay buffer [1× Dulbecco's PBS containing 0.9 mM Ca^{2+}, 0.5 mM Mg^{2+}, 25 mM D-glucose, and 100 mM HEPES (pH 7.0)]. Permeability to p28 and TMZ was measured in 2 directions: The apical (A) to basolateral (B) direction (influx) and the B to A direction (efflux). For the drug transport assays, the BBB model inserts were transferred to other wells containing prewarmed assay buffers. As specified in the assay kit directions, the medium in the donor compartment of the BBB model was replaced with medium containing 10 μM p28 (N = 3) or 100 μM TMZ (N = 2). The concentration of TMZ was chosen based on its pharmacokinetic property in metastatic melanoma patients.[40] Relatively similar concentration of p28 (100 μM TMZ = 20 μg/mL, 20 μg/mL of p28 = ~10 μM) was used in the assay. The plate was incubated for 30 minutes at 37°C, following which the samples were collected from the acceptor compartment and quantitatively analyzed by LC/MS.[41] Medium without any test compounds was used as blank control. The apparent permeability (Papp) coefficients (cm/sec) were calculated according to the following formula:

$$\text{Papp} = (dC/dT \times V) / (A \times C_0)$$

where dC/dt represents the change in concentration in the basal chamber (μg/s), V is the volume (mL) of the basal chamber, A is the membrane surface area (cm^3), and C_0 is the initial concentration in the apical chamber at 0 minutes. The efflux ratio, defined as Papp(B–A)/Papp(A–B), was used to estimate the magnitude of efflux.

Colony Formation Assay

MDA-231BR and Mel-7 cells were seeded in 6-well plates at a density of 1000 cells per well and incubated at 37°C overnight. MDA-231BR and Mel-7 cells were exposed to 50 μM p28 or 0.5 Gy irradiation (IR) alone or in combination. In another set of experiments, Mel-7 cells were also treated with 50 μM p28 or 100 μM TMZ alone, or in combination. Fifty μM Scrambled-p28 (Scr) was used as a negative control peptide. Cesium-137 irradiator (JL Shephard) and TMZ doses that inhibited 20% cell proliferation (IC_{20}) were used. Cells cultured in the media without any treatment were used as a control. The medium was replaced with fresh growth medium containing the indicated treatment 3 times a week, and the cells were incubated at 37°C for a total of 2 weeks. Then, the cells were fixed with 4% paraformaldehyde and stained with 2% methylene blue. Colony size less than 2 mm were disregarded.

Apoptosis Assay

MDA-231BR and Mel-7 cells were seeded in 10 cm dishes and cultured overnight. MDA-MB231BR and Mel-7 cells were treated with 50 μM p28 or 0.5 Gy IR or in combination. Mel-7 cells were also treated with 50 μM p28 or 100 μM TMZ or in combination. Apoptotic cells were detected by using Apoptosis kits (Life Technologies, #V13242). After 24 hours, the cells were washed with 1X PBS, detached with TrypLE (Gibco), and collected by centrifugation. Then, the cells were washed and resuspended with 1X annexin binding buffer, and the cell density was adjusted to 1 × 10^6 cells/mL. Subsequently, 5 μL of annexin-V was added to 100 μL of cell suspension, and the mixture was incubated for 15 minutes at room temperature. The cells were washed, incubated with 5 μL of PI (propidium iodide) for an additional 15 minutes on ice, washed, resuspended in 200 μL of buffer, and subjected to flow cytometry (Gallios flow cytometer). Kaluza software was used to analyze the proportions of dead (top left quadrant), late apoptotic (top right quadrant), early apoptotic (bottom right quadrant), and viable (bottom left quadrant) cells. Untreated cells were used as controls.

Western Blotting

Whole-cell lysates were prepared in RIPA buffer containing protease inhibitors (Cell Signaling Technology, #9806S). Mitochondrial and cytosolic proteins were extracted following the instructions of the Mitochondria Isolation Kit (Fisher, #89874). Briefly, the cells were incubated on ice with Reagent A for 2 minutes. Then, Reagent B was added, and the cells were incubated on ice for 5 minutes with vortexing every minute. After Reagent C was added, the samples were centrifuged at 700 × g for 10 minutes at 4°C, and the supernatant was collected and centrifuged at 12 000 × g for 15 minutes at 4°C. The resulting supernatant, which contained the cytosolic fraction, was collected in a new tube, and the pellet, which contained the mitochondrial fraction, was washed with Reagent C. The protein concentrations in the lysates were determined using Bradford reagent (BioRad, #500-0006). The cellular proteins were denatured, separated by 4%–12% SDS–PAGE, And transferred to nitrocellulose membranes, which were probed with antibodies against the following proteins: p53 (Santa Cruz Biotechnology, #SC-17846), p21 (Santa Cruz Biotechnology, #SC-397), Cyclin A (Biosource, #AHF0022), Cyclin E (Biosource, #AHF0312), CDK1 (Santa Cruz Biotechnology, #SC-53219), CDK2 (Santa Cruz Biotechnology, #SC-163), ATP5a (Santa Cruz Biotechnology, #SC-136178) and actin (Santa Cruz Biotechnology, #SC-1616). Anti-actin and anti-ATP5a antibodies were used as loading controls.[42] All antibodies were used at 1:1000 dilution. Western blot detection was performed using the ECL assay kit (ThermoFisher Scientific, # 34577).

Construction of BM Mouse Models by Intracardiac Injection

All animal experiments were approved by the Animal Care and Use Committee of University of Illinois and were performed in accordance with the Guide for the Care and Use of Laboratory Animals. Four- to five-week-old athymic

nude mice were purchased from The Jackson Laboratory. Subconfluent MDA-MB231BR was fed fresh medium 24 hours before preparation for intracardiac injection. Cells were harvested with 0.2% EDTA and 0.02% trypsin, incubated in the culture medium, and suspended in PBS immediately before heart inoculation. The female mice were anesthetized with ketamine/xylazine i.p. and placed in the supine position. A 30-gauge needle was inserted into the left ventricle of the heart, and after confirming the withdrawal of fresh arterial blood, cell suspensions (100 000 cells/0.1 mL PBS/mouse) were slowly injected as described previously.[43] Mouse was monitored for recovery by maintaining its body temperature from the heat pad and was subsequently transferred to the colony room.

In Vivo Imaging of Indocyanine Green (ICG)-Labeled p28 (ICG-p28)

Once the tumors in mice were confirmed by MRI, they received an intravenous injection of 0.5 mg/kg ICG-p28.[41,44] Twenty-four hours later, near-infrared (NIR) images of brains were obtained by the Odyssey system (LI-COR, NE) and the FDA 510(k)-cleared NIR imaging system PDE neo (Photodynamic Eye; Mitaka USA, UT) as described previously.[41,44] Specific NIR signals at 800 nm were recorded.

In Vivo Bioluminescence Assay

MDA-231BR cells stably expressing the luciferase gene (pGL4.51[luc2/CMV/Neo], Promega) were generated by chemical transfection (FuGENE HD, Promega) in the presence of G418 (GoldBio). The presence of metastases in mice intracardially injected with MDA-231BR-luc cells was assessed at various time points after tumor cell injection using noninvasive bioluminescence imaging. Briefly, mice received an intraperitoneal injection of 200 μL of 15 mg/mL D-luciferin potassium salt (GoldBio, #LUCK-100; the final dose of 150 mg/kg). Then, the mice were anesthetized in a chamber containing 2% isoflurane and oxygen and positioned for bioluminescent imaging using a Spectral Lago X imaging system. A series of images were acquired over 30 minutes after the D-luciferin injection. Aura software (version 3.2) was used to identify the regions of interest and integrate the total bioluminescence signal in each ROI. Data for each ROI were analyzed using radiance (photons/s/cm^2/steradian).

Histological Analysis

Collected brain samples were fixed in buffered 3.7% formalin (Anatech) for 24 hours, after which the formalin was replaced with 70% ethanol. The samples were embedded in paraffin, and the paraffin blocks were cut into 4 μm-thick sections and mounted on slides for hematoxylin and eosin (H&E) staining and Ki67 staining.[44]

Statistical Analysis

GraphPad Prism 9.0 was used for the statistical analysis of data. Two-tailed *t*-tests were used for single comparison, and group differences were evaluated using ANOVA. Data were presented as means±SEM, and all experiments were performed in triplicates unless otherwise mentioned.

Results

p28 Crosses the BBB In Vitro

As the target diseases are BMs in this study, we first quantitatively investigated the ability of p28 to cross the BBB in an in vitro 3D model. In this model, the apical side represents the blood, and the basolateral side represents the brain, and permeability (Papp) was measured in 2 directions, from apical to basolateral (A–B, influx) and from basolateral to apical (B–, efflux) (Figure 1A). In general, the Papp(A–B) of CNS-positive compounds ranges from 3.4 × 10^{-6} cm/seconds to 20.2 × 10^{-6} cm/sec, with a threshold of 3 × 10^{-6} cm/seconds 45. CNS-positive compounds exhibit a low Papp(B–A) or an efflux rate of less than 2.5.[45] For p28 with this model, the Papp(A–B) was 5 × 10^{-6} cm/seconds, and the Papp(B–A) was only 0.9 × 10^{-6} cm/seconds ($P < .0001$, Figure 1B). This result indicates the efficient influx of p28 across the BBB with low efflux. To better understand the potential implication of these Papp values, we compared the permeability of the in vitro BBB model to p28 and the standard chemotherapeutic TMZ, which is known to cross the BBB.[46] The influx of p28 was significantly higher than that of TMZ (2.67 × 10^{-6} cm/seconds) ($P < .001$, Figure 1C). Thus, these findings suggest that p28 crosses the BBB with a high influx rate and is thus a potent CNS drug candidate.

p28 Crosses the Intact BBB and Preferentially Localizes to Tumor Lesions In Vivo

Given the initial indication that p28 can cross the BBB, we first confirmed p28 preferentially penetration into cancer cells in vitro (Figure 2A). We next aimed to confirm this result in an in vivo model. As the most common types of cancer that form BMs are breast cancer, lung cancer, and melanoma, we used cell lines of these cancer types to generate mouse models of BMs with which to assess p28 entry into the CNS.[4] To avoid disrupting the BBB, we introduced melanoma, breast cancer, and lung cancer cell lines into athymic mice via intracardiac injection. BMs were detected by T_2-weighted MRI of the brain. Some of the mice developed BMs 4–6 weeks after the injection of Mel-7 (60%, 3/5 mice), MDA-231BR (100%, 5/5 mice), BCA-1 (80%, 4/5 mice), or A549 (60%, 3/5 mice) cells into the left cardiac ventricle (Supplementary Figure 1). Moreover, these mice showed signs of BMs, including severe clinical and neurological symptoms such as body weight loss, behavioral changes, and paralysis (Supplementary Movies). We created BM mouse models of breast cancer, lung cancer, and melanoma without using stereotactic implantation.

Next, we investigated BBB permeability and the preferential localization of p28 in the BM models with such cancer cells. ICG-p28[41,44] was intravenously injected into the BM model mice, and p28 localization was assessed with NIR fluorescence. Upon systemic administration, ICG-p28

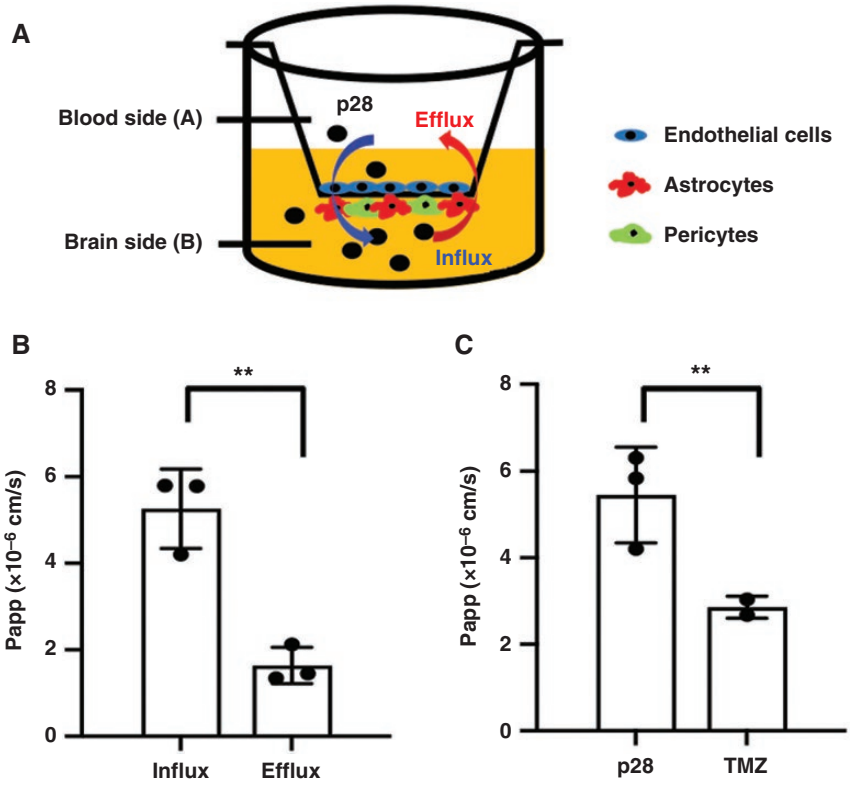

Figure 1. p28 crosses the blood-brain barrier (BBB) in an in vitro 3D model. (A) Schematic of the in vitro 3D BBB model. Human brain vascular endothelial cells were cultured in the upper chamber of the Transwell system, and pericytes and astrocytes were cultured in the bottom chamber to form 2 distinct cell layers that mimic the transport properties of the BBB. (B) The apical (A) to basolateral (B) (influx) and B to A (efflux) transport of p28. (C) Permeability (influx) of p28 and TMZ in the BBB model. Mean ± SEM, ** $P < .01$.

successfully crossed the BBB and localized to lesions in the brain, which were confirmed to be tumors by H&E staining (Figure 2B). Along with the earlier in vitro data, these in vivo data suggest that p28 readily crosses the intact BBB and preferentially localizes to and is retained in tumor lesions in the brain.

p28 Sensitizes BMs to DNA-Damaging Agents In Vitro

Non-small cell lung cancer is the most common type of lung cancer, and most cases of Non-Small Cell Lung Cancer are adenocarcinomas.[47] Patients with melanoma and breast cancer have shorter overall survival than those with lung adenocarcinoma.[48] Here, we focused on and examined whether p28 can enhance the effects of standard treatments for BM [irradiation (IR) and TMZ] on MDA-231BR breast cancer cells with a point mutation in p53 gene (R280K)[23] and Mel-7 melanoma cells carrying wild type p53.[49] In MDA-231BR cells, radiation in combination with p28 significantly decreased colony formation compared to PBS (73% reduction), Scrambled-p28 (Scr) (75% reduction), p28 alone (70% reduction), and radiation alone (64% reduction) (Figure 3A). Similarly, colony formation of Mel-7 cells significantly decreased after treatment with TMZ in combination with p28 compared to treatment with PBS (70% reduction), Scrambled-p28 (Scr) (74% reduction), p28 alone (59% reduction), or TMZ alone (60% reduction) (Figure 3B). Treatment of Mel-7 cells with radiation in combination with p28 significantly decreased colony formation compared to treatment with PBS (71% reduction), Scrambled-p28 (Scr) (67% reduction), p28 alone (51% reduction), or radiation alone (49% reduction) (Figure 3C). Together, the findings suggest that p28 enhances the pharmacological effect of DNA-damaging agents, TMZ, or IR.

To investigate the effects of these treatment combinations on apoptosis, MDA-231BR cells were treated with p28 or radiation alone or in combination, and Mel-7 cells were treated with p28 or TMZ alone or radiation alone or in combination with p28; flow cytometric analysis with annexin V-PI staining was used to assess apoptosis. The percentage of apoptotic MDA-231BR cells significantly increased after treatment with radiation in combination with p28 compared to treatment with p28 alone and radiation alone (Figures 3D, E). Compared with p28 or TMZ alone, the combination of p28 and TMZ significantly increased apoptosis in Mel-7 cells (Figures 3F, G). Treatment of Mel-7 cells with the combination of p28 and radiation significantly increased the apoptotic cell percentage as compared to p28 or radiation alone (Figures 3H, I). These results show that p28 in combination with radiation or TMZ decreases colony formation by increasing apoptosis.

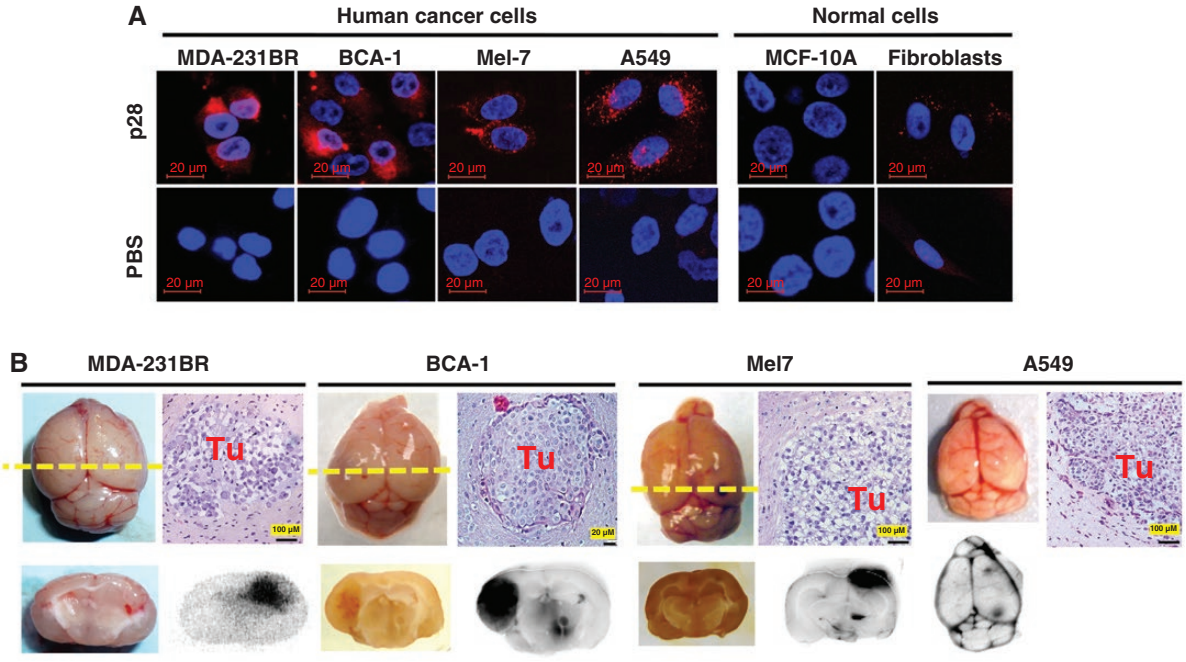

Figure 2. p28 crosses the BBB and preferentially localizes to Brain metastases (BMs). (A) Confocal images of the penetration of normal and cancer cells by p28. Human cancer cell lines (MDA-231BR, BCA-1, Mel-7, and A549) and normal cells (MCF-10A and fibroblasts) were cultured with Alexa Fluor 568-labeled p28 at 37°C for 2 hours, and images were obtained by confocal microscopy. Red, p28; blue, DAPI (nucleus). (B) MDA-231BR brain-specific metastatic triple-negative breast cancer, BCA-1 breast cancer, Mel-7 melanoma, or A549 lung cancer cells were injected into the left cardiac ventricle of athymic mice. ICG-labeled p28 was intravenously injected into the mice. Near-infrared fluorescence imaging of the ICG-p28 signal (gray) in coronal brain sections (yellow dotted line on the anterior-dorsal view) of mice injected with MDA-231BR, BCA-1 or Mel-7 cells or in the anterior-dorsal view of the brain of mice injected with A549 cells. H&E staining of brain sections confirmed the presence of BMs (Tu).

p28 Enhances the Effect of DNA-Damaging Agents by Modulating the p53-p21 Axis

One of the master regulators of the cellular response to DNA damage is the tumor suppressor p53.[50] Upon exposure to radiation or the alkylating agent TMZ, the DNA damage response is activated, which increases p53 levels, leading to cell-cycle arrest and activation of the intrinsic apoptosis pathway.[50] p28 can inhibit the cell cycle by blocking the proteasomal degradation of p53, resulting in its stabilization in cancer cells.[23] Moreover, based on the KEGG pathway analyses[51] in melanoma and breast cancer, the p53 pathway was identified (Supplementary Figure 2). Therefore, we examined the effect of combination treatment on the p53 pathway in MDA-231BR and Mel-7 cells. Western blot analyses showed that p53 levels substantially increased in response to single-agent treatment with p28, IR, or TMZ (Figure 4A). More importantly, the protein levels of p53 and its downstream CDK inhibitor p21 were significantly higher in cells treated with p28 and IR or TMZ than in cells treated with a single agent (Figure 4A). To gain more insight into the mode of action of the combination therapies, the levels of cell-cycle- and apoptosis-related proteins were determined. The levels of cyclin A, CDK1, and CDK2, but not of cyclin E, were decreased in both MDA-231BR and Mel-7 cells exposed to p28 in combination with radiation or TMZ compared to cells treated with PBS, p28 alone, or DNA-damaging agent alone (Figure 4A). Additionally, cytochrome c (Cyt c) release from mitochondria was assessed, as this intrinsic apoptosis-related process contributes to apoptosome complex formation, which subsequently leads to apoptosis.[52] As expected, Cyt c release into the cytoplasm of MDA-231BR and Mel-7 cells increased upon exposure to each individual agent (p28, IR, or TMZ) (Figure 4B). Notably, MDA-231BR and Mel-7 cells treated with p28 in combination with radiation or TMZ showed increased Cyt c levels in the cytosolic fraction but decreased Cyt c levels in the mitochondrial fraction (Figure 4B), suggesting the induction of apoptosis. Collectively, these data demonstrate that p28 enhances the activity of DNA-damaging agents such as radiation and TMZ by modulating the p53-p21 axis.

Combination Treatment With p28 Increases the Antitumor Activity of Radiation in a BM Mouse Model

To investigate the in vivo relevance of the cellular findings, mice with confirmed BMs formed by injected MDA-231BR cells were treated with radiation alone or in combination with p28 for 30 days. Due to its greater susceptibility to the combination approach (Figure 3A), luciferase-expressing MDA-231BR was created and used

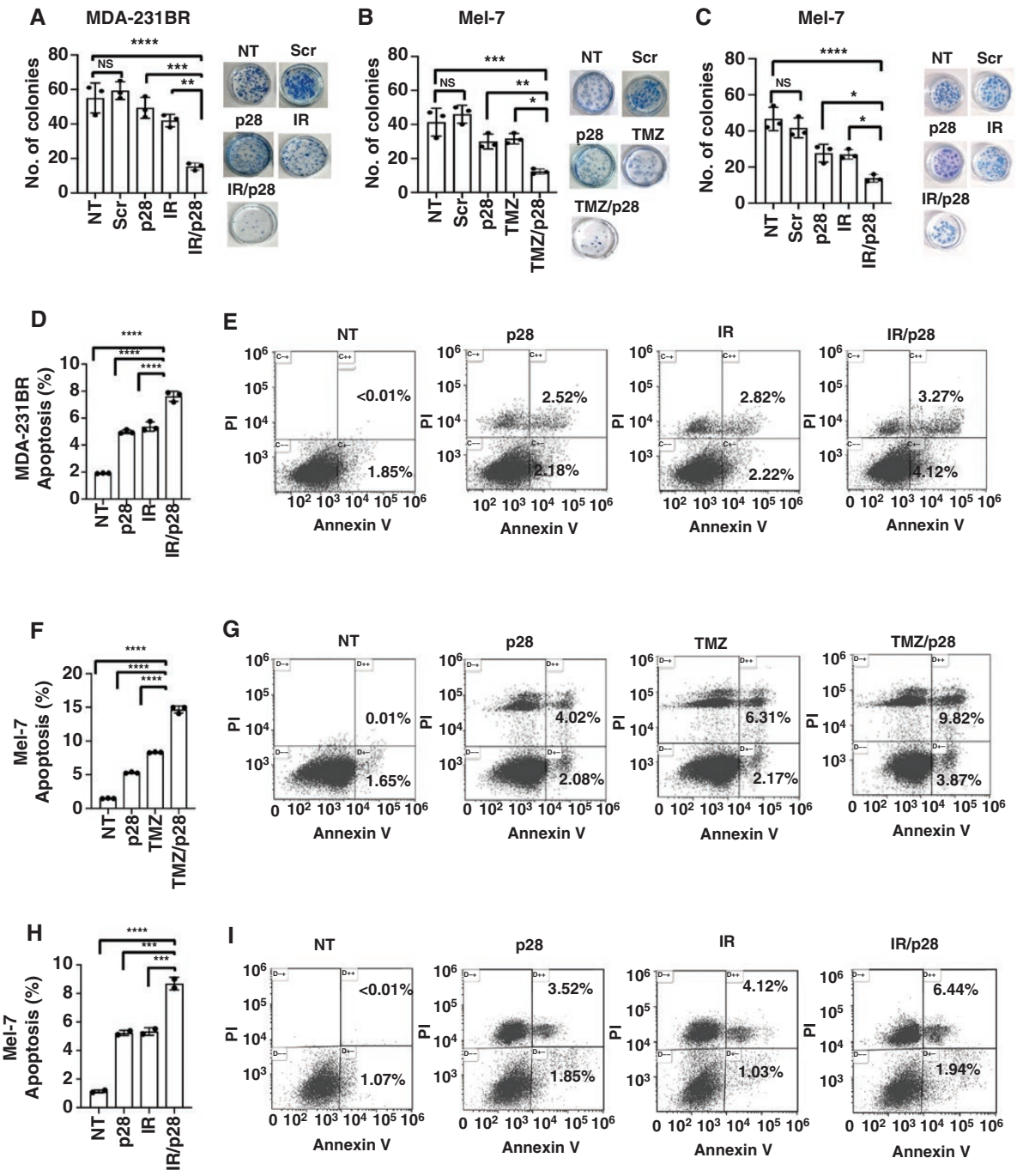

Figure 3. p28 enhances the effects of radiation and TMZ. (A) Colonies were counted after MDA-231BR cells were treated with 50 μM p28 or 0.5 Gy radiation (IR) alone or in combination for 2 weeks. 50 μM Scrambled-p28 (Scr) was used as a control. Data are presented as the number of colonies per well, with representative images shown at the top. $N = 3$ per group. (B) Mel-7 cells were treated with 50 μM p28 or 100 μM TMZ alone or in combination and analyzed as described for (A). (C) Mel-7 cells were treated with 50 μM p28 or 0.5 Gy radiation (IR) alone or in combination and analyzed as described for (A). The percentage of apoptotic MDA-231BR (D, E) and Mel-7 (F, G, H, I) cells was quantitatively measured by flow cytometry. Data are presented as the mean±SEM. * $P < .05$, ** $P < .01$, *** $P < .001$, and **** $P < .0001$ (ANOVA).

in this study. Mice in the control group were euthanized at an earlier time point (day 20) due to the tumor burden in the brain. Bioluminescence images showed that compared with the control, radiation alone suppressed tumor growth, as expected (Figures 5A, B). Beginning 1 week after treatment initiation and continuing through week 4, combination treatment with p28 and radiation significantly suppressed tumor growth compared to radiation alone, as observed in representative images and indicated by quantitation (Figures 5A, B). These in vivo results confirm the in

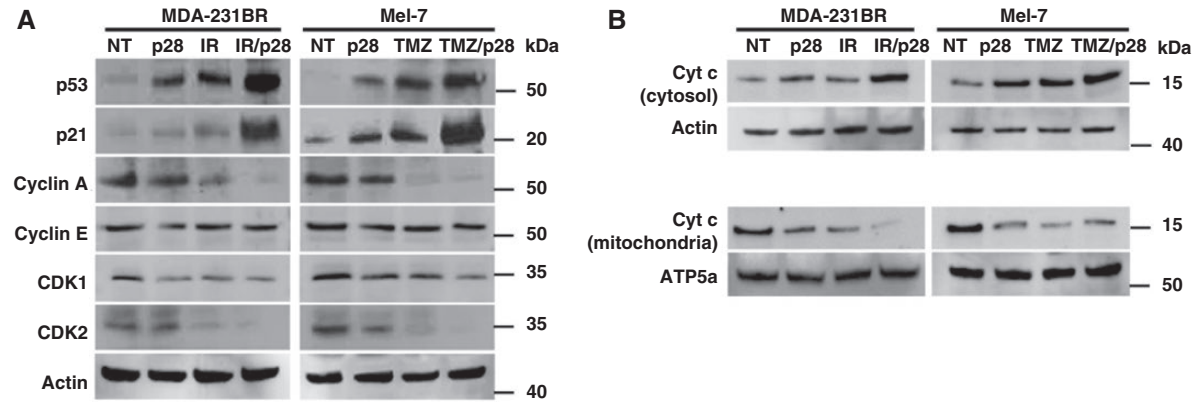

Figure 4. Induction of the p53-p21 axis. (A, B) MDA-231BR cells were exposed to PBS (NT), p28, radiation (IR), or the combination of p28 and radiation (p28/IR) for 24 hours (left panel). Mel-7 cells were exposed to p28, TMZ, or p28/TMZ for 24 hours (right panel). Proteins from whole-cell lysates (A) or from mitochondrial and cytosolic fractions (B) were separated by NuPAGE, and the indicated proteins were detected by western blotting. Actin and ATP5a were used as loading controls.

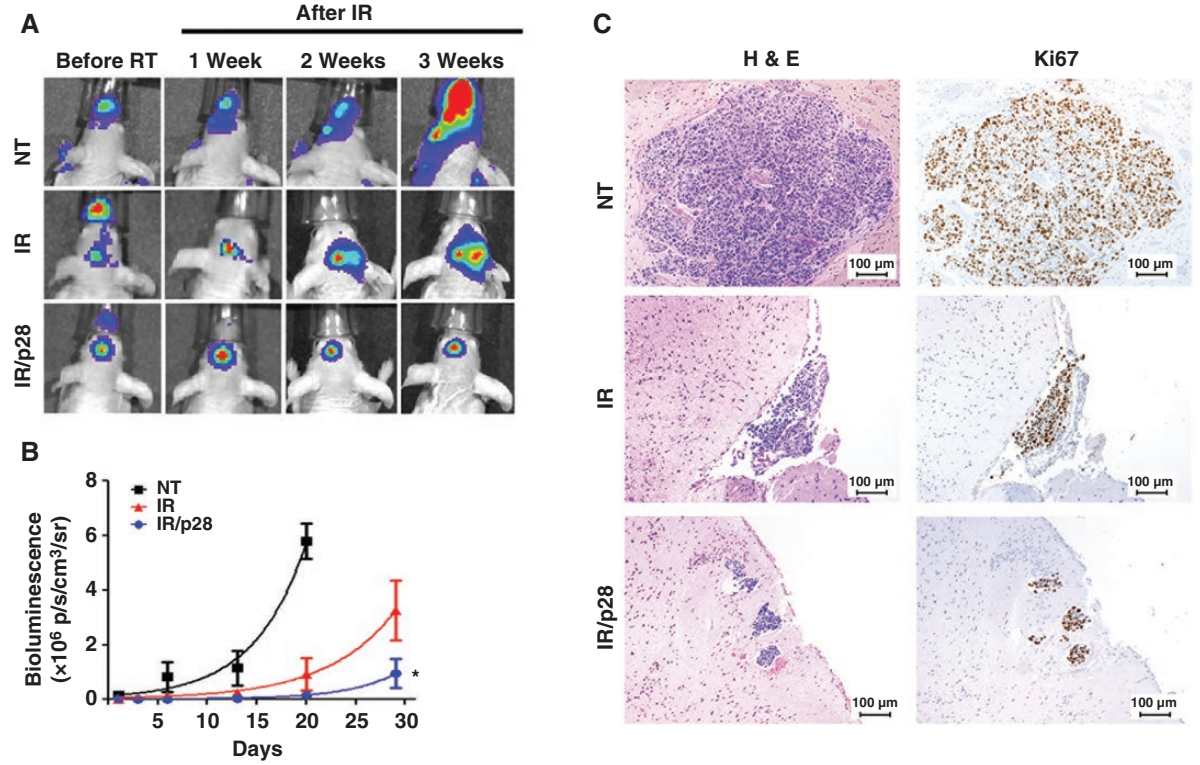

Figure 5. p28 enhances the effect of radiation in a BM mouse model. MDA-231BR human triple-negative breast cancer cells stably expressing the luciferase gene (MDA-231BR-luc cells) were injected into the left cardiac ventricle of female athymic mice. After the development of brain metastases was confirmed, the animals were randomly divided into 3 groups. (A) Representative images of bioluminescence in the mice before and 1, 2, and 3 weeks after treatment with radiation (IR) alone or in combination with p28. (B) Quantitation of bioluminescence. Control: $N = 5$; IR alone: $N = 10$; p28/IR: $N = 10$. Mean±SEM. * $P = .05$ (IR alone vs. p28/IR). (C) Histological analysis of brain sections from representative mice in each group. Paraffin-embedded brain sections were stained with H&E and for the proliferation marker Ki67.

vitro findings that p28 and radiation in combination have a greater inhibitory effect on tumors than single-agent treatment. To confirm the decrease in tumor burden in the brain, immunohistochemistry (IHC) was used to visualize cancer cells within the brains of mice in the control, radiation, and radiation in combination with p28 groups. H&E staining showed the presence of large tumors in the brains of mice in the control group, whereas mice treated with

radiation alone or in combination with p28 had smaller tumors (Figure 5C). The cells within the brain lesions were identified as highly proliferative cancer cells based on Ki67 staining (Figure 5C). These results showed that p28 can readily cross the intact BBB, localize to tumor lesions in the brain and enhance the antitumor effects of radiation on BMs.

Discussion

Radiation therapy plays an essential role in the management of BMs.[53] While surgical and radio-surgical techniques have evolved over the past decades, improvements in targeted chemotherapy have begun to offer benefits for patients with certain cancer types.[54,55] The major factors that regulate the response to chemotherapy are the drug sensitivity of the primary tumor and BMs and the BBB permeability to the agent.[56] TMZ has been used widely in the treatment of glioblastoma and BMs owing to its ability to penetrate the BBB.[57] Successful treatment of BM requires agents to both selectively target the tumor and penetrate the BBB.[58] Drug uptake by the brain is limited by several factors, including the BBB and efflux transport systems.[59] Brain endothelial cells, pericytes, astrocytes, neurons, and the basal membrane form the tight physical barrier of the BBB, which allows the selective passage of gases and certain molecules while restricting the passage of most other molecules.[60] Efflux transporters in the BBB act as additional obstacles to the entry of substances into the brain.[61] Many therapeutic agents for brain cancer are ineffective because they are unable to cross the BBB despite the use of various invasive and noninvasive administration techniques.[62,63] Among the recent advances in delivery systems, the transport of therapeutic molecules into the CNS through CPP-based delivery systems appears to hold considerable promise due to the excellent ability of these systems to efficiently carry macromolecules across cellular membranes with minimal cell toxicity.[14] Our in vitro and in vivo data revealed that p28 has the ability to cross the BBB. The apparent permeability of p28 across the BBB is 5×10^{-6} cm/seconds, which is similar to a CNS-targeting drug diazepam (5.20×10^{-6} cm/seconds),[64] significantly greater than that of TMZ (2.67×10^{-6} cm/seconds), and greater than the threshold for candidate CNS drugs (3×10^{-6} cm/seconds).[45] Our BBB permeability result for TMZ (2.67×10^{-6} cm/seconds) was similar (2.7×10^{-6} cm/seconds) to the previous report.[65] In metastatic melanoma patients, the pharmacokinetic profile showed that C_{max} reached ~20 μg/mL when patients received 200 mg/m^{2}TMZ.[40] With the relatively similar doses of TMZ and p28 in the 3D BBB assay, BBB permeability of p28 was significantly higher, suggesting the different mechanisms of BBB penetration. The transport efficiency of compounds across the BBB is dependent on several factors such as lipophilicity (TMZ: lipophilic, p28: Amphipathic properties)[46,66] and molecular weight (TMZ: 194.15 g/mol, p28: 2,918 g/mol). It has been suggested that TMZ enters and exits cells via passive diffusion without undergoing any specialized membrane transport processes.[65,67] Although we demonstrated that p28 can enter endothelial cells (lesser than cancer cells) though, at least in part, endocytosis via caveosomes,[68] a further mechanistic study on BBB penetration is needed.

The BBB presents an obstacle to the passage of both solutes and cells into the brain. For cancer cells to metastasize to the brain, they must undergo morphological changes and cross the BBB, which constitutes the endothelium and surrounding cells.[69] It is important to use an appropriate preclinical mouse model that successfully recapitulates the biological characteristics of BMs. It is not surprising that many preclinical findings from animal studies fail to reflect the complexity of metastases in humans and that drug responses in models with a compromised BBB cannot be validated in human clinical trials.[70] In this study, we constructed BMs mouse models by intracardial injection of the most common cancer types (breast cancer, lung cancer, and melanoma) that form BMs. These mouse models develop BMs without disruption of the BBB, unlike those constructed by the stereotactic injection method. Recent studies have demonstrated that nerve growth factor receptor (NGFR/CD271) is crucial for melanoma cells survival, migration, stemness, and cellular plasticity and has been found to drive the progression of melanoma BMs.[71] In this study, we found CD271 upregulation in Mel-7 from melanoma brain metastasis as compared to the primary site tumor cells (Supplementary Figure 3), suggesting that our animal model, at least in part, confers the neural characteristics of melanoma BMs. In experiments with these BMs models, p28 was found to cross the BBB and preferentially accumulate in BMs lesions.

In summary, we report the therapeutic potential of p28 in combination with DNA-damaging agents such as radiation and TMZ in vitro and in appropriate animal models and provide mechanistic insight into how p28 enhances the effects of DNA-damaging agents. Our study provides a clear rationale for the use of combination approaches involving the brain-penetrant molecule p28 for the treatment of BMs.

Supplementary material

Supplementary material is available online at *Neuro-Oncology* (http://neuro-oncology.oxfordjournals.org/).

Keywords:

brain metastases | blood-brain barrier | cell-penetratin peptide | combination therapy | targeted delivery

Funding

This research was supported in part by the National Institutes of Health/ National Cancer Institute (R21CA252370) and the National Institutes of Health/ National Institute of Biomedical Imaging and Bioengineering (R01EB023924) to TY.

Acknowledgment

This work made use of the Biological Resources Laboratory and Research Resource Core facilities (Radiation, Preclinical Imaging-MRI and IVIS, Flow cytometry, and Fluorescence Imaging) at UIC. MDA-231BR cells were a kind gift from Dr. T. Yoneda, The University of Texas Health Science Center at San Antonio.

Conflict of interest statement

The authors report no conflict of interest.

Authorship statement

Conceptualized and designed the experiments: SM, TKDG, TY. Performed experiments: SM, GSG, LUC, KC, AG, TY. Analyzed experiments: SM, GSG, KC. Data interpretation: SM, KC, TKDG, TY. Manuscript writing, review, and edits: SM, GSG, LUC, KC, AG, TKDG, TY.

Data availability statement

The data used in this study are available from the corresponding author upon reasonable request. All relevant data are included in this article and its supplementary information.

References

1. Achrol AS, Rennert RC, Anders C, et al. Brain metastases. *Nat Rev Dis Primers.* 2019;5(1):5.
2. Posner JB, Chernik NL. Intracranial metastases from systemic cancer. *Adv Neurol.* 1978;19(1):579–592.
3. Takakura K, Watanabe T. [Immunotherapy of brain tumors]. *No Shinkei Geka.* 1982;10(12):1245–1254.
4. Nayak L, Lee EQ, Wen PY. Epidemiology of brain metastases. *Curr Oncol Rep.* 2012;14(1):48–54.
5. O'Beirn M, Benghiat H, Meade S, et al. The expanding role of radiosurgery for brain metastases. *Medicines (Basel).* 2018;5(3).
6. Sperduto PW, Kased N, Roberge D, et al. The effect of tumor subtype on the time from primary diagnosis to development of brain metastases and survival in patients with breast cancer. *J Neurooncol.* 2013;112(3):467–472.
7. Barnholtz-Sloan JS, Yu C, Sloan AE, et al. A nomogram for individualized estimation of survival among patients with brain metastasis. *Neuro Oncol.* 2012;14(7):910–918.
8. Tan AC, Ashley DM, López GY, et al. Management of glioblastoma: State of the art and future directions. *CA Cancer J Clin.* 2020;70(4):299–312.
9. Caruso G, Raudino G, Caffo M. Patented nanomedicines for the treatment of brain tumors. *Pharm Pat Anal.* 2013;2(6):745–754.
10. Lockman PR, Mittapalli RK, Taskar KS, et al. Heterogeneous blood-tumor barrier permeability determines drug efficacy in experimental brain metastases of breast cancer. *Clin Cancer Res.* 2010;16(23):5664–5678.
11. Oller-Salvia B, Sánchez-Navarro M, Giralt E, Teixidó M. Blood-brain barrier shuttle peptides: An emerging paradigm for brain delivery. *Chem Soc Rev.* 2016;45(17):4690–4707.
12. Mendonça DA, Bakker M, Cruz-Oliveira C, et al. Penetrating the blood-brain barrier with new peptide-porphyrin conjugates having anti-HIV activity. *Bioconjug Chem.* 2021;32(6):1067–1077.
13. Wu L-P, Ahmadvand D, Su J, et al. Crossing the blood-brain-barrier with nanoligand drug carriers self-assembled from a phage display peptide. *Nat Commun.* 2019;10(1):4635.
14. Cavaco M, Valle J, da Silva R, et al. (D)PepH3, an improved peptide shuttle for receptor-independent transport across the blood-brain barrier. *Curr Pharm Des.* 2020;26(13):1495–1506.
15. Frankel AD, Pabo CO. Cellular uptake of the tat protein from human immunodeficiency virus. *Cell.* 1988;55(6):1189–1193.
16. Banks WA. Peptides and the blood-brain barrier. *Peptides.* 2015;72:16–19. doi: 10.1016/j.peptides.2015.03.010
17. Raucher D, Ryu JS. Cell-penetrating peptides: Strategies for anticancer treatment. *Trends Mol Med.* 2015;21(9):560–570.
18. Hyun S, Lee Y, Jin SM, et al. Oligomer formation propensities of dimeric bundle peptides correlate with cell penetration abilities. *ACS Cent Sci.* 2018;4(7):885–893.
19. Habault J, Poyet JL. Recent advances in cell penetrating peptide-based anticancer therapies. *Molecules.* 2019;24(5):927.
20. Yamada T, Fialho AM, Punj V, et al. Internalization of bacterial redox protein azurin in mammalian cells: Entry domain and specificity. *Cell Microbiol.* 2005;7(10):1418–1431.
21. Choi JK, Naffouje SA, Goto M, et al., Cross-talk between cancer and Pseudomonas aeruginosa mediates tumor suppression. *Commun Biol.* 2023;6(1):16.
22. Taylor BN, Mehta RR, Yamada T, et al. Noncationic peptides obtained from azurin preferentially enter cancer cells. *Cancer Res.* 2009;69(2):537–546.
23. Yamada T, Christov K, Shilkaitis A, et al. p28, A first in class peptide inhibitor of cop1 binding to p53. *Br J Cancer.* 2013;108(12):2495–2504.
24. Yamada T, Das Gupta TK, Beattie CW. p28-mediated activation of p53 in G2-M phase of the cell cycle enhances the efficacy of DNA damaging and antimitotic chemotherapy. *Cancer Res.* 2016;76(8):2354–2365.
25. Jia L, Gorman GS, Coward LU, et al. Preclinical pharmacokinetics, metabolism, and toxicity of azurin-p28 (NSC745104) a peptide inhibitor of p53 ubiquitination. *Cancer Chemother Pharmacol.* 2011;68(2):513–524.
26. Warso MA, Richards JM, Mehta D, et al. A first-in-class, first-in-human, phase I trial of p28, a non-HDM2-mediated peptide inhibitor of p53 ubiquitination in patients with advanced solid tumours. *Br J Cancer.* 2013;108(5):1061–1070.
27. Lulla RR, Goldman S, Yamada T, et al. Phase I trial of p28 (NSC745104), a non-HDM2-mediated peptide inhibitor of p53 ubiquitination in pediatric patients with recurrent or progressive central nervous system tumors: A Pediatric Brain Tumor Consortium Study. *Neuro Oncol.* 2016;18(9):1319–1325.
28. Daphu I, Sundstrøm T, Horn S, et al. In vivo animal models for studying brain metastasis: Value and limitations. *Clin Exp Metastasis.* 2013;30(5):695–710.
29. Steeg PS. Targeting metastasis. *Nat Rev Cancer.* 2016;16(4):201–218.
30. Lowery FJ, Yu D. Brain metastasis: Unique challenges and open opportunities. *Biochim Biophys Acta Rev Cancer.* 2017;1867(1):49–57.
31. Balathasan L, Beech JS, Muschel RJ. Ultrasonography-guided intracardiac injection: An improvement for quantitative brain colonization assays. *Am J Pathol.* 2013;183(1):26–34.

32. Geisler JA, Spehar JM, Steck SA, et al. Modeling brain metastases through intracranial injection and magnetic resonance imaging. *J Vis Exp.* 2020(160). doi: 10.3791/61272
33. Zhang RD, Price JE, Fujimaki T, Bucana CD, Fidler IJ. Differential permeability of the blood-brain barrier in experimental brain metastases produced by human neoplasms implanted into nude mice. *Am J Pathol.* 1992;141(5):1115–1124.
34. On NH, Savant S, Toews M, Miller DW. Rapid and reversible enhancement of blood-brain barrier permeability using lysophosphatidic acid. *J Cereb Blood Flow Metab.* 2013;33(12):1944–1954.
35. Wyatt EA, Davis ME. Method of establishing breast cancer brain metastases affects brain uptake and efficacy of targeted, therapeutic nanoparticles. *Bioeng Transl Med.* 2019;4(1):30–37.
36. Ireson CR, Alavijeh MS, Palmer AM, Fowler ER, Jones HJ. The role of mouse tumour models in the discovery and development of anticancer drugs. *Br J Cancer.* 2019;121(2):101–108.
37. Aldape K, Brindle KM, Chesler L, et al. Challenges to curing primary brain tumours. *Nat Rev Clin Oncol.* 2019;16(8):509–520.
38. Rauth S, Kichina J, Green A, Bratescu L, Das Gupta TK. Establishment of a human melanoma cell line lacking p53 expression and spontaneously metastasizing in nude mice. *Anticancer Res.* 1994;14(6b):2457–2463.
39. Mehta RR, Bratescu L, Graves JM, et al. Human breast carcinoma cell lines: ultrastructural, genotypic, and immunocytochemical characterization. *Anticancer Res.* 1992;12(3):683–692.
40. Plummer ER, Middleton MR, Jones C, et al. Temozolomide pharmacodynamics in patients with metastatic melanoma: DNA damage and activity of repair enzymes O6-alkylguanine alkyltransferase and poly(ADP-ribose) polymerase-1. *Clin Cancer Res.* 2005;11(9):3402–3409.
41. Naffouje SA, Goto M, Coward LU, et al. Nontoxic tumor-targeting optical agents for intraoperative breast tumor imaging. *J Med Chem.* 2022;65(10):7371–7379.
42. Jezek J, Chang KT, Joshi AM, Strich R. Mitochondrial translocation of cyclin C stimulates intrinsic apoptosis through Bax recruitment. *EMBO Rep.* 2019;20(9):e47425.
43. Yoneda T, Williams PJ, Hiraga T, Niewolna M, Nishimura R. A bone-seeking clone exhibits different biological properties from the MDA-MB-231 parental human breast cancer cells and a brain-seeking clone in vivo and in vitro. *J Bone Miner Res.* 2001;16(8):1486–1495.
44. Goto M, Ryoo I, Naffouje S, et al. Image-guided surgery with a new tumour-targeting probe improves the identification of positive margins. *EBioMedicine.* 2022;76:103850. doi: 10.1016/j.ebiom.2022.103850
45. Wang Q, Rager JD, Weinstein K, et al. Evaluation of the MDR-MDCK cell line as a permeability screen for the blood-brain barrier. *Int J Pharm.* 2005;288(2):349–359.
46. Agarwala SS, Kirkwood JM. Temozolomide, a novel alkylating agent with activity in the central nervous system, may improve the treatment of advanced metastatic melanoma. *Oncologist.* 2000;5(2):144–151.
47. Chen Z, Fillmore CM, Hammerman PS, Kim CF, Wong KK. Non-small-cell lung cancers: A heterogeneous set of diseases. *Nat Rev Cancer.* 2014;14(8):535–546.
48. Sperduto PW, Mesko S, Li J, et al. Survival in patients with brain metastases: summary report on the updated diagnosis-specific graded prognostic assessment and definition of the eligibility quotient. *J Clin Oncol.* 2020;38(32):3773–3784.
49. Kichina JV, Rauth S, Das Gupta TK, Gudkov AV. Melanoma cells can tolerate high levels of transcriptionally active endogenous p53 but are sensitive to retrovirus-transduced p53. *Oncogene.* 2003;22(31):4911–4917.
50. Lee CL, Blum JM, Kirsch DG. Role of p53 in regulating tissue response to radiation by mechanisms independent of apoptosis. *Transl Cancer Res.* 2013;2(5):412–421.
51. Kabir F, Apu MNH. Multi-omics analysis predicts fibronectin 1 as a prognostic biomarker in glioblastoma multiforme. *Genomics.* 2022;114(3):110378110378.
52. Kim HE, Du F, Fang M, Wang X. Formation of apoptosome is initiated by cytochrome c-induced dATP hydrolysis and subsequent nucleotide exchange on Apaf-1. *Proc Natl Acad Sci U S A.* 2005;102(49):17545–17550.
53. Schiff D, Messersmith H, Brastianos PK, et al. Radiation therapy for brain metastases: ASCO guideline endorsement of ASTRO guideline. *J Clin Oncol.* 2022;40(20):.JCO.22.00333.
54. Venur VA, Ahluwalia MS. Targeted therapy in brain metastases: ready for primetime? *Am Soc Clin Oncol Educ Book.* 2016;35(36):e123–e130.
55. Brastianos PK, Galanis E, Butowski N, et al. Advances in multidisciplinary therapy for meningiomas. *Neuro Oncol.* 2019;21 (suppl 1):i18–i31. doi: 10.1093/neuonc/noy136
56. Daneman R, Prat A. The blood-brain barrier. *Cold Spring Harb Perspect Biol.* 2015;7(1):a020412a020412.
57. Giorgio CG, Giuffrida D, Pappalardo A, et al. Oral temozolomide in heavily pre-treated brain metastases from non-small cell lung cancer: Phase II study. *Lung Cancer.* 2005;50(2):247–254.
58. Osswald M, Solecki G, Wick W, Winkler F. A malignant cellular network in gliomas: Potential clinical implications. *Neuro Oncol.* 2016;18(4):479–485.
59. Graff CL, Pollack GM. Drug transport at the blood-brain barrier and the choroid plexus. *Curr Drug Metab.* 2004;5(1):95–108.
60. Pehlivan SB. Nanotechnology-based drug delivery systems for targeting, imaging and diagnosis of neurodegenerative diseases. *Pharm Res.* 2013;30(10):2499–2511.
61. Löscher W, Potschka H. Drug resistance in brain diseases and the role of drug efflux transporters. *Nat Rev Neurosci.* 2005;6(8):591–602.
62. Kadry H, Noorani B, Cucullo L. A blood–brain barrier overview on structure, function, impairment, and biomarkers of integrity. *Fluids Barriers CNS.* 2020;17(1):69.
63. Gregory JV, Kadiyala P, Doherty R, et al. Systemic brain tumor delivery of synthetic protein nanoparticles for glioblastoma therapy. *Nat Commun.* 2020;11(1):5687.
64. Heymans M, Sevin E, Gosselet F, Lundquist S, Culot M. Mimicking brain tissue binding in an in vitro model of the blood-brain barrier illustrates differences between in vitro and in vivo methods for assessing the rate of brain penetration. *Eur J Pharm Biopharm.* 2018;127:453–461. doi: 10.1016/j.ejpb.2018.03.007
65. Zhou Q, Gallo JM. Differential effect of sunitinib on the distribution of temozolomide in an orthotopic glioma model. *Neuro Oncol.* 2009;11(3):301–310.
66. Signorelli S, Santini S, Yamada T, et al. Binding of amphipathic cell penetrating peptide p28 to wild type and mutated p53 as studied by Raman, atomic force and surface plasmon resonance spectroscopies. *Biochim Biophys Acta Gen Subj.* 2017;1861(4):910–921.
67. Seo S, Nah S-Y, Lee K, Choi N, Kim HN. Triculture model of in Vitro BBB and its application to study BBB-associated chemosensitivity and drug delivery in glioblastoma. *Adv Funct Mater.* 2022;32(10):2106860.
68. Mehta RR, Yamada T, Taylor BN, et al. A cell penetrating peptide derived from azurin inhibits angiogenesis and tumor growth by inhibiting phosphorylation of VEGFR-2, FAK and Akt. *Angiogenesis.* 2011;14(3):355–369.
69. Abbott NJ, Rönnbäck L, Hansson E. Astrocyte-endothelial interactions at the blood-brain barrier. *Nat Rev Neurosci.* 2006;7(1):41–53.
70. Hidalgo M, Amant F, Biankin AV, et al. Patient-derived xenograft models: An emerging platform for translational cancer research. *Cancer Discov.* 2014;4(9):998–1013.
71. Radke J, Schumann E, Onken J, et al. Decoding molecular programs in melanoma brain metastases. *Nat Commun.* 2022;13(1):7304.